Acta Astronautica 138 (2017) 394–406

Contents lists available at ScienceDirect

Acta Astronautica

journal homepage: www.elsevier.com/locate/actaastro

# Thermodynamic efficiency analysis and cycle optimization of deeply precooled combined cycle engine in the air-breathing mode

Jianqiang Zhang [a,b], Zhenguo Wang [a,b,*], Qinglian Li [a,b]

[a] College of Aerospace Science and Engineering, National University of Defense Technology, Changsha, Hunan 410073, People's Republic of China
[b] Science and Technology on Scramjet Laboratory, National University of Defense Technology, Changsha, Hunan 410073, People's Republic of China

ARTICLE INFO

*Keywords:*
SABRE
Component-level modeling
Cycle efficiency
Exergy analysis
Cycle optimization
Helium recirculation scheme

ABSTRACT

The efficiency calculation and cycle optimization were carried out for the Synergistic Air-Breathing Rocket Engine (SABRE) with deeply precooled combined cycle. A component-level model was developed for the engine, and exergy efficiency analysis based on the model was carried out. The methods to improve cycle efficiency have been proposed. The results indicate cycle efficiency of SABRE is between 29.7% and 41.7% along the flight trajectory, and most of the wasted exergy is occupied by the unburned hydrogen in exit gas. Exergy loss exists in each engine component, and the sum losses of main combustion chamber(CC), pre-burner(PB), precooler(PC) and 3# heat exchanger(HX3) are greater than 71.3% of the total loss. Equivalence ratio is the main influencing factor of cycle, and it can be regulated by adjusting parameters of helium loop. Increase the maximum helium outlet temperature of PC by 50 K, the total assumption of hydrogen will be saved by 4.8%, and the cycle efficiency is advanced by 3% averagely in the trajectory. Helium recirculation scheme introduces a helium recirculation loop to increase local helium flow rate of PC. It turns out the total assumption of hydrogen will be saved by 9%, that's about 1740 kg, and the cycle efficiency is advanced by 5.6% averagely.

## 1. Introduction

Air-breathing combined cycle engines have been rapidly developed to enable the reusable vehicles [1]. With the implementation of inlet-air cooling, the operation range of the air-breathing mode engine could be extended to Mach 6 with increased specific impulse [2]. Synergistic Air-Breathing Rocket Engine (SABRE) is a revolutionary deeply precooled combined cycle engine, characterized by both a great thrust as rocket engine and a high specific impulse as aircraft engine [1–3]. SABRE can be operated on dual-modes. In the air-breathing mode, it works like a turbojet engine with the air as the oxidant; when the aircraft reaches an altitude of 26 km with speed of Mach 5, it changes into rocket engine mode and climbs out of the atmosphere rapidly. The engine was first proposed by Reaction Engine Ltd. (REL) in 1989 as propulsion system the SKYLON project, which is designed to be a single-stage-to-orbit reusable spaceplane [3–5].

SABRE have attracted wide attentions [6–11] and big progresses on the key technologies have been obtained by REL [12–16]. For example, the ground experiment of PC has succeeded in 2012, and the company has thrown daylight on the plan of 1/4 scaling demonstration engine. The engine appears promising. However, there is scarce practical knowledge about the engine to the public. Some of the literature emphasize on the engine concept only [8,10,17], and few quantitative calculations are reported [18–20]. Víctor and Guillermo [18,19] developed a model for a high speed propulsion system with EcosimPro and the European Space Propulsion Simulation System. A full simulation has been done to compute the performance of SABRE during its air-breathing trajectory and the variation of thrust and specific impulse was yielded [18]. They also focused on the scimitar engine, which derived from SABRE and made some change with the cycle to fulfill different mission. A dynamic numerical model was developed for the engine along a determined trajectory between Mach 2.5 and 5. The thrust and specific impulse were detailed [19]. Moreover, the cycle efficiency has been evaluated according to the exergy analysis [21].

In generally, there are no much performance calculations of SABRE, especially on the cycle analysis, which is helpful for understanding of the engine. The operation characteristics of engine can be obtained by the cycle analysis, including the variation of cycle parameters, cycle efficiency and loss distribution. After all, the cycle analysis is necessary for both assessment and optimization of the engine. Exergy analysis is an important method for cycle analysis of engine, and it has been used widely for the aircraft engine, rocket engine and scramjet [21–29].

* Corresponding author. College of Aerospace Science and Engineering, National University of Defense Technology, Changsha, Hunan 410073, People's Republic of China.
*E-mail address:* Zhenguo_Wang@nudt.edu.cn (Z. Wang).

http://dx.doi.org/10.1016/j.actaastro.2017.06.011
Received 29 March 2017; Received in revised form 31 May 2017; Accepted 10 June 2017
Available online 15 June 2017

**Nomenclature**

*Abbreviation*

| | |
|---|---|
| AC | air compressor |
| BB | bypass burner |
| CC | main combustion chamber |
| CE | core engine |
| HeC | helium circulator |
| HeT | helium turbine |
| HeV | helium valve |
| HT1 | hydrogen turbine1 |
| HT2 | hydrogen turbine2 |
| HT3 | hydrogen turbine3 |
| HV | hydrogen valve |
| HX1 | 1# heat exchanger |
| HX2 | 2# heat exchanger |
| HX3 | 3# heat exchanger |
| HX4 | 4# heat exchanger |
| HX5 | 5# heat exchanger |
| LHP | liquid hydrogen pump |
| LHT | liquid hydrogen tank |
| PB | pre-burner |
| PC | pre-cooler |
| PRV | pressure reduction valve |
| RC | recirculator |
| REL | Reaction Engine Ltd |
| SABRE | Synergistic Air-Breathing Rocket Engine |

*Variables*

| | |
|---|---|
| $A$ | area |
| $C_m$ | coupling coefficient of conversion mass flow rate |
| $C_\pi$ | coupling coefficient of pressure ratio |
| $C_\eta$ | coupling coefficient of efficiency |
| $Cp$ | specific heat at constant pressure |
| $Ex$ | exergy |
| $Ex_c$ | chemistry exergy |
| $Ex_e$ | effective exergy |
| $Ex_k$ | kinetic exergy |
| $Ex_p$ | potential exergy |
| $Ex_{ph}$ | physical exergy |
| $Ex_q$ | heat exergy |
| $F$ | thrust |
| $h$ | specific enthalpy |
| $Is$ | specific impulse |
| $k$ | specific heat ratio |
| $M$ | mass |
| $\dot{m}$ | mass flow rate |
| $n$ | rotating speed |
| $P$ | pressure |
| $Q$ | heat transfer rate |
| $T$ | temperature |
| $v$ | velocity |
| $W$ | work |
| $\eta$ | efficiency |
| $\pi$ | pressure ratio |
| $\rho$ | density |
| $\Delta Ex$ | exergy loss |
| $\Delta P$ | pressure difference |
| $\Delta T$ | temperature difference |

*Subscripts*

| | |
|---|---|
| *amb* | ambient |
| *c* | compressor |
| *e* | exit |
| *in* | inlet |
| *max* | maximum |
| *out* | outlet |
| *p* | turbopump |
| *sep* | separate point |
| *t* | turbine |

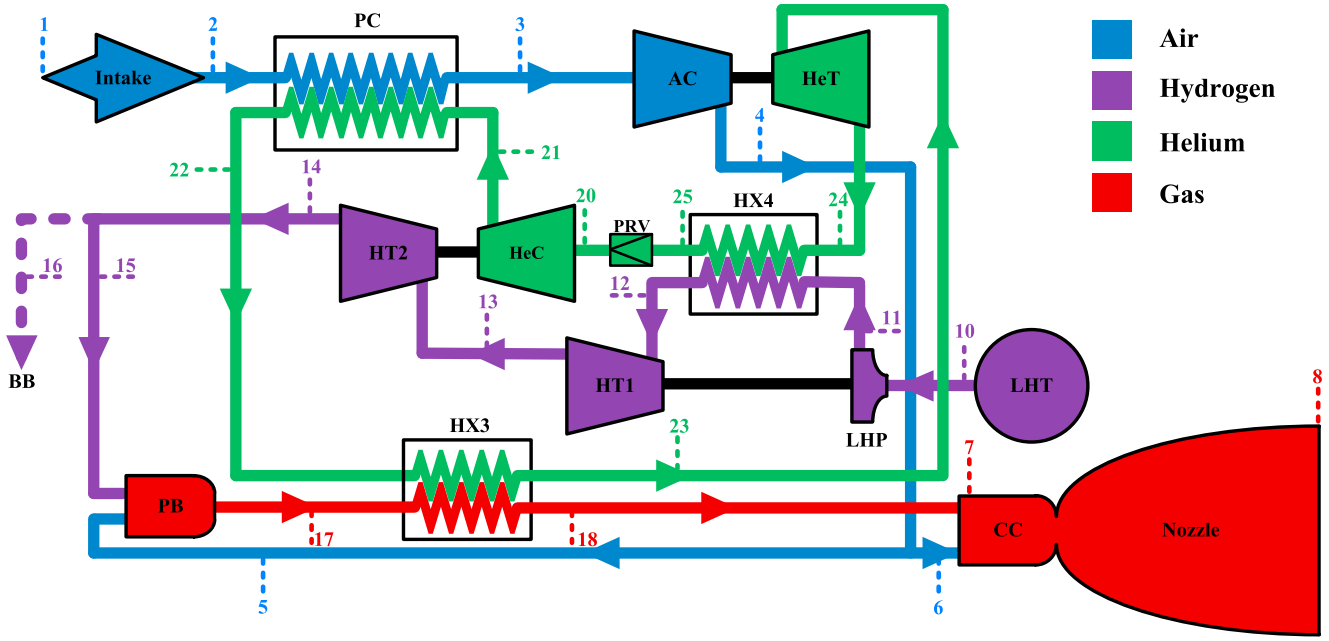


**Fig. 1.** Thermodynamic cycle schematic of SABRE in air-breathing mode.

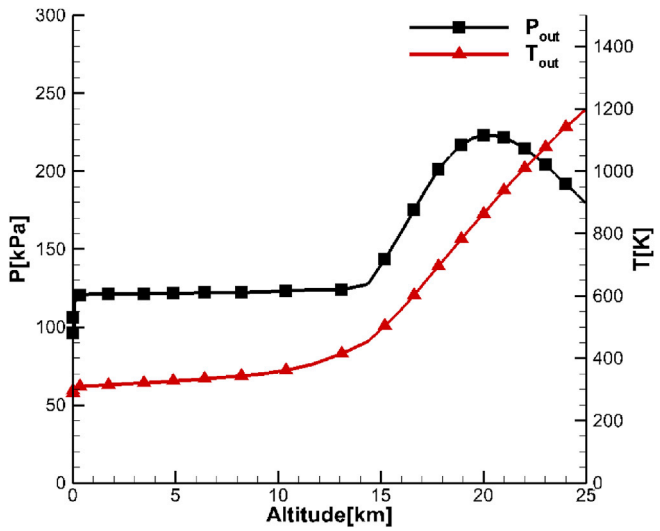


**Fig. 2.** Outlet recovery parameters of SABRE intake [12].

The paper develops a component-level model [30–32] to calculate SABRE performance in the air-breathing mode, which is widely applied in the research and development of aircraft engine. Based on the model, exergy analysis of the engine is carried out for the first time. The exergy flow and loss of each component are detailed along the trajectory. At last, methods for the cycle optimization are proposed and the validation calculation has been completed. The paper is helpful to deepen understanding of the engine working process, and it could play a significant role in improving engine performance.

## 2. Component-level modeling of SABRE

### 2.1. Target engine

Fig. 1 is a diagram of SABRE cycle in the air-breathing mode. SABRE is composed of the core engine (CE) and bypass burner (BB). The present study is focused on performance of CE, which is composed of the intake, heat exchanger, compressor, turbine, pump, combustion chamber, nozzle and so on. As shown in the figure, CE introduces Brayton cycle between air and liquid hydrogen with helium as the medium. After the primary compression in the intake, the airstream is deeply cooled to about −140 °C by helium in PC and then is further compressed to a pressure level of rocket thrust chamber in air compressor (AC). Then the airstream is separated into two parts. One part is fed into pre-burner (PB) to react with the liquid hydrogen fuel; the other part is fed into main combustion chamber (CC) to react with the fuel-rich product from the PB. Liquid hydrogen is pumped into 4# heat exchanger (HX4) and vaporized, then it drives 1# hydrogen turbine (HT1) and 2# hydrogen turbine (HT2) before entering PB. The high temperature gas from PB heats up helium in 3# heat exchanger (HX3) and enters CC finally. Helium drives helium turbine (HeT) after heat absorption in PC and HX3, then be cooled to the initial low temperature by liquid hydrogen in HX4, and continues the cycle beginning with helium circulator (HeC). After changing to the rocket mode, the engine adopts the single series of combustion chamber, nozzle and pump, which lighten the weight effectively. Therefore, SABRE is the most appropriate propulsion system for single-stage-to-orbit spaceplane up to the present.

### 2.2. Component-level model

In order to evaluate the performance of SABRE, a component-level model is developed for CE. The method is based on accurate model of each component, and integrates all of these components through system equations [33]. In the design state, parameters of all the components are confirmed; then in the off-design state, the cooperating point of all the components can be obtained by solving the system equations, meanwhile performance of the whole engine can be calculated.

#### 2.2.1. The control law of engine

According to the data in Refs. [2,3,12,18], the following control laws are adopted in the engine design:

1) The helium loop is configured with a PRV to adjust the loop pressure, as shown in Fig. 1;
2) Liquid hydrogen is pumped into CE and BB. At sea level, BB does not work and its liquid hydrogen flow rate is zero. Above the sea level, BB is switched on and the corresponding liquid hydrogen flow rate remains constant;
3) Inlet helium temperature of HeT $T_{in,HeT}$ is constant, and maintains at 1080 K [2];
4) The helium outlet temperature of PC $T_{22}$ is limited to 950 K due to material temperature limitation [15].

The paper calculates the thrust produced by CE, taking no account of the drag introduced by intake and the thrust produced by BB. The

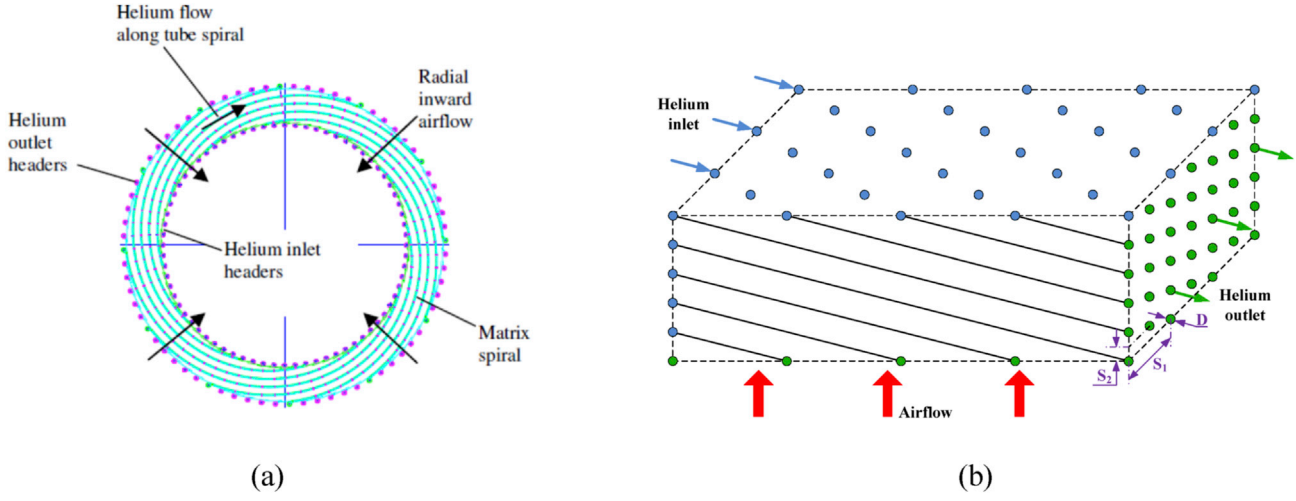


**Fig. 3.** Structure sketch of PC, (a) frontal view of the module [16], (b) equivalent matrix of tubes in airflow.

following assumptions are made in the calculation:

1) Ignore the flow loss of pipeline and heat transfer between components and environment;
2) The physical parameters of working fluids change along with temperature and pressure, and the data are obtained through database of National Institute of Standards and Technology.

*2.2.2. The main component model*

The following description gives a general overview of the elements adopted in the component model. More information can be found in Refs. [12,34–36].

*2.2.2.1. Intake.* The inlet pressure and temperature are determined by the flight altitude and Mach number. Airflow through the intake can be considered as an adiabatic compression process. By determining a total pressure recovery coefficient, the temperature and pressure at the intake outlet could be obtained as the functions of flight altitude. Fig. 2 shows the outlet temperature and pressure of intake along the flight trajectory in the REL design [12]. The curve is selected in the present study.

*2.2.2.2. Heat exchanger.* PC is a shell and tube heat exchanger (cf. Fig. 3a), and the tube bundle is in staggered arrangement (cf. Fig. 3b). Air flows through the tube bundle in shell side, while helium flows in the tube. Heat exchange between air and helium include three processes: heat convection between air and outside wall of tube, heat conduction of the tube and heat convection between helium and inside wall of tube, of which the heat resistance is $R_o$, $R_{tube}$ and $R_i$ respectively.

The main parameters of the heat exchanger, heat transfer rate Q and pressure drop $\Delta P$, can be calculated as [35,37].

$$\begin{cases} Q = \dfrac{\Delta T \cdot A}{R} = \dfrac{\Delta T \cdot A}{R_o + R_{tube} + R_i} \\ \Delta P = \xi \cdot \dfrac{\rho v^2}{2} = f(\mathrm{Re}, d, D, S_1, S_2, l, z) \cdot \dfrac{\rho v^2}{2} \end{cases} \tag{1}$$

where $\Delta T$, $R$, $\xi$, Re, $d$, $D$, $S_1$, $S_2$, $l$, $z$ denote temperature difference, heat resistance, flow resistance coefficient, Reynolds number, inner diameter, external diameter, transverse tube spacing, vertical tube spacing, tube length and tube row number.

The performances of other heat exchangers (e.g., HX3, HX4 and so on) are simplified, with the effectiveness to be assumed as constant and the flow loss to be ignored.

*2.2.2.3. Turbomachinery.* Since the engine is still in the pre-research stage, there are no available parameters to determine the performance of the turbomachinery. The performance for the turbomachinery are determined based on a reference turbomachinery from Ref. [33]. The calculation introduces the concept of coupling coefficient, including $C_m$, $C_\pi$ and $C_\eta$ for conversion mass flow rate, pressure ratio and efficiency respectively (see Eq. (2)). The coupling coefficient is introduced as the scaling factor when the parameters are proportionally changed to overlap the design point of new engine and the existing characteristic curve.

$$\begin{cases} C_m = \dfrac{\dot{m}_{d,cor}}{\dot{m}'_{d,cor}} \\ C_\pi = \dfrac{\pi_d - 1}{\pi'_d - 1} \\ C_\eta = \dfrac{\eta_d}{\eta'_d} \end{cases} \Rightarrow \begin{cases} \dot{m}_{cor} = C_m \dot{m}'_{cor} \\ \pi = C_\pi(\pi' - 1) + 1 \\ \eta = C_\eta \eta' \end{cases} \tag{2}$$

The off-design parameters of the new turbomachinery can be obtained by the inverse process of calculating coupling coefficient, as shown in Eq. (2), wherein the subscript "d" denotes design state and the superscript "′" denotes the reference turbomachinery.

$$\begin{cases} \text{compresso} \begin{cases} P_{out} = P_{in} \cdot \pi \\ h_{out} = h_{in} + \dfrac{(h_{out,id} - h_{in})}{\eta} \end{cases} \\ \text{turbine} \begin{cases} P_{out} = \dfrac{P_{in}}{\pi} \\ h_{out} = h_{in} - (h_{in} - h_{out,id})\eta \end{cases} \end{cases} \tag{3}$$

The outlet parameters can be calculated by Eq. (3), wherein the ideal parameters are obtained according to the isentropic theory. Ignore the mechanical loss of shaft.

*2.2.2.4. Turbopump.* For a specified pump, the outlet parameters can be calculated by Eq. (4), wherein n denotes rotating speed and $\bar{\rho}$ is the average density of fluid in inlet and outlet.

$$\begin{cases} (P_{out}, T_{out}) = f_1(\dot{m}, n, P_{in}, T_{in}, \bar{\rho}) \\ \bar{\rho} = f_2(P_{in}, T_{in}, P_{out}, T_{out}) \end{cases} \tag{4}$$

It is indicated that the outlet parameters such as pressure, temperature and density are coupled and should be calculated through the iterations [38]. The calculation ignores the speed of fluid in the inlet and outlet.

*2.2.2.5. Combustion chamber.* There are two combustion chambers (cf. PB and CC) in the system. The pressure drop, $\Delta P_{injection}$, is set as 40% of the chamber pressure (see Eq. (5)). Neglecting the total pressure loss and heat loss of the combustion chamber, the combustion process can be considered as an isobaric adiabatic process [3,34,36,39]. The combustion process is calculated by an open source software, Cantera [37], with the assumption of chemical reaction equilibrium [40].

$$\begin{cases} P_c = P_{in} - \Delta P_{injection} \\ \Delta P_{injection} = 0.4 P_c \end{cases} \tag{5}$$

*2.2.2.6. Nozzle.* The nozzle performance is determined based on the adiabatic equilibrium assumption. The gas compositions do not change during the expansion process. The inlet loss, friction loss, expansion loss and losses induced by boundary layer are ignored. The thrust could be calculated as [36]:

$$F = \begin{cases} \dot{m} v_e + (P_e - P_{atm}) A_e & if: P_e > 0.215 P_{atm} \\ \dot{m} v_{sep} + (P_{sep} - P_{atm}) A_{sep} + \xi_{sep} (P_{sep} - P_{atm}) (A_e - A_{sep}) & if: P_e \le 0.215 P_{atm} \end{cases} \tag{6}$$

When ambient pressure $P_{amb}$ is much higher than the designed exit pressure $P_{e,d}$, the gas flow separates in the nozzle. The calculation process can be found in Ref. [34]. The separation pressure $P_{sep}$ is chosen to be

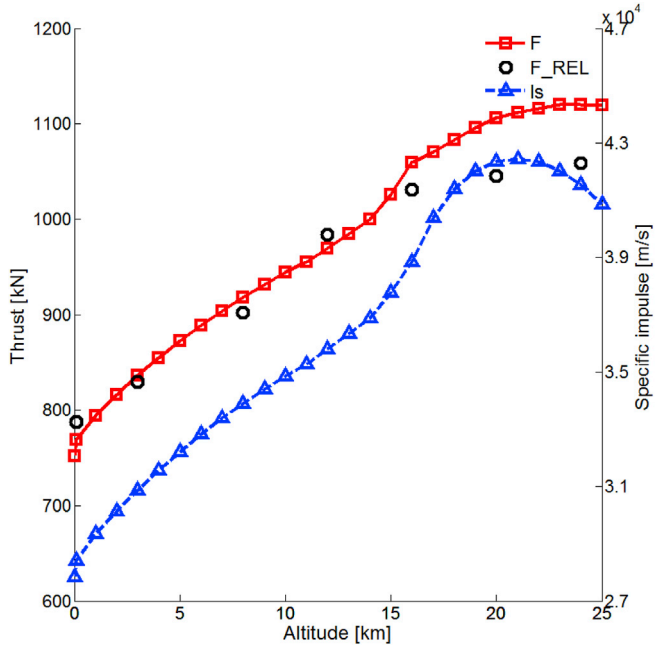


**Fig. 4.** Variation of thrust *F* and specific impulse *Is* along the fight trajectory.

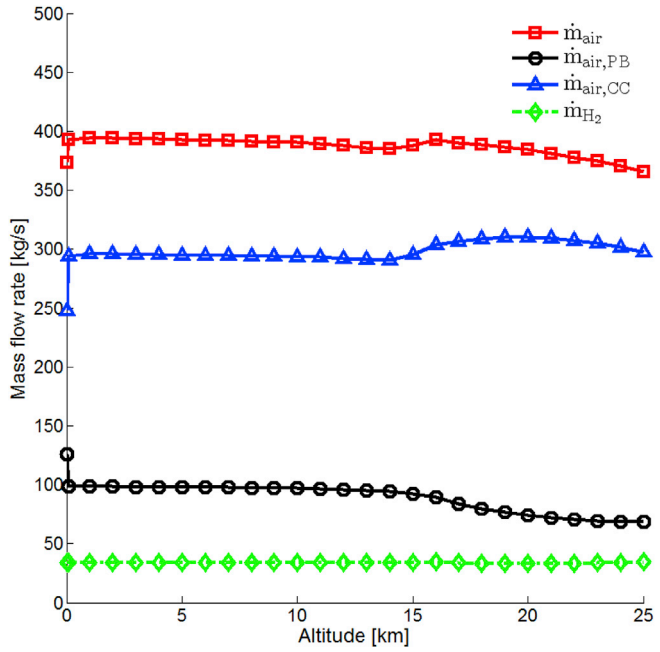


**Fig. 5.** Variation of mass flow rate of propellants along the fight trajectory.

0.215 $P_{amb}$. $\xi_{sep}$ stands for the pressure restoration ratio, which is between 0.1 and 0.5.

*2.2.2.7. PRV.* The helium loop is equipped with a PRV at the inlet of HeC, and it can maintain a pressure balance by regulating the opening of PRV. The calculation does not consider the specific adjustment process of PRV, and it works as long as the inlet pressure of PRV is greater than that of HeC. Assume that helium flows through PRV as an isenthalpic process (see Eq. (7)).

$$h_{out}(P_{out}, T_{out}) = h_{in}(P_{in}, T_{in}) \tag{7}$$

### 2.2.3. System equations

The specific system equations are shown in Eq. (8), wherein the number of subscripts indicates the position marked in Fig. 1. The meanings of these numbers of subscripts are the same in the following sections.

$$\begin{cases} E(1) = (\dot{m}_3 - \dot{m}_2)/\dot{m}_2 \\ E(2) = (W_{AC} - W_{HeT})/W_{HeT} \\ E(3) = (W_{LHP} - W_{HT1})/W_{HT1} \\ E(4) = (W_{HeC} - W_{HT2})/W_{HT2} \\ E(5) = (\dot{m}_{23} - \dot{m}_{20})/\dot{m}_{20} \\ E(6) = (\dot{m}_{12} - \dot{m}_{10})/\dot{m}_{10} \\ E(7) = (\dot{m}_{13} - \dot{m}_{10})/\dot{m}_{10} \\ E(8) = (T_{25} - T_{20})/T_{20} \\ E(9) = (T_{23} - T_{in,HeT})/T_{in,HeT} \\ E(10) = (P_4 - P_{15})/P_{15} \\ E(11) = (\dot{m}_8 - \dot{m}_7)/\dot{m}_7 \\ E(12) = P_{25} - P_{20} \geq 0 \end{cases} \tag{8}$$

In Eq. (8), E(1)~E(11) are the equality constraints and E(12) is the inequality constraint that inlet pressure of PRV is greater than that of HeC. Optimization of objective function method is used to solve the functions. The objective function is $fo = \sum_{i=1}^{11} |E(i)|$, and the convergence criteria of the optimization is $fo \leq 2e-5$.

### 2.3. Model evaluation

An altitude of 25 km with flight speed of Mach 4.86 is selected as the design point, and the detailed operation parameters are listed in Fig. 7(a). Then the performance variation of the engine is calculated along the trajectory.

For the design point, the thrust is 1119 kN and specific impulse is 40876 m/s. Therefore SABRE is an engine with both a large thrust as rocket engines and a high specific impulse as aircraft engines. The inlet pressure of helium PRV is 4.2 MPa, higher than the initial pressure (i.e. 3 MPa). Thus it is necessary to adjust the opening degree of PRV to achieve the pressure balance of helium loop.

Fig. 4 shows the variation of thrust and specific impulse along the flight trajectory. It is shown that the predicted thrust agrees well with the data published by REL, with a maximum error less than 6%. The developed component-level model is verified to be accurate, and it can be used to calculate the cycle parameters of SABRE along the trajectory. As the altitude increases, the thrust becomes larger and the variation tends to slow down when above 15 km. The specific impulse increases firstly. And after reaching the maximum of about 42448 m/s at the altitude of 21 km, the specific impulse begins to decrease, with a value greater than 27800 m/s along the entire trajectory.

Fig. 5 shows the variation of mass flow rate of the propellants along the flight trajectory, and Fig. 6 is curves of pressure and temperature of combustion chamber. Air flow rate increases rapidly when the spaceplane takes off from sea level. This is because the recovery total pressure of intake has a jump after taking off (cf. Fig. 2). As the altitude increased, mass flow rate of liquid hydrogen changes slightly. Meanwhile, air flow rate into PB decreases in order to maintain $T_{in,HeT}$ to be constant. Therefore temperature of PB and CC decreases and increases respectively. The pressure of PB is equal to that of CC and changes slightly around the design point of 10.4 MPa.

The detailed cycle parameters (see Fig. 7(a)) can be obtained along the trajectory, which is the base of exergy analysis in the following section.

## 3. Exergy analysis of the cycle

Based on the component-level model in Section 2, the second law of thermodynamics is applied to analyze utilization and loss of exergy in the cycle process [41]. The method directs at the actual cycle process, so the results are insured with credibility and accuracy.

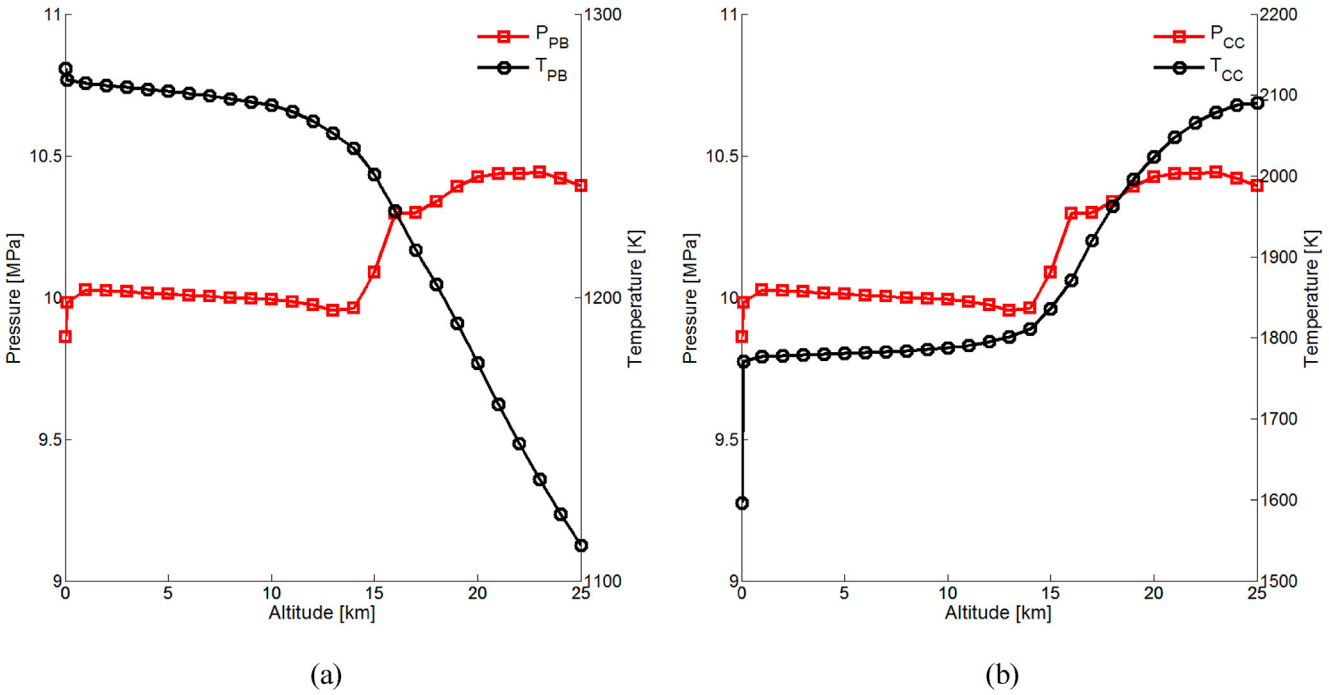


**Fig. 6.** Variation of pressure and temperature of: (a) PB and (b) CC, along the fight trajectory.

### 3.1. Exergy analysis method

Exergy of system under a certain state is defined to be the maximum power when it changes to the ground state. The present study employs herein Kameyama-Yoshida environment model [42] to calculate exergy. For a steady and stable process with no nuclear, magnetic, electrical and surface tension effects, the exergy consists of kinetic exergy $Ex_k$, potential exergy $Ex_p$, physical exergy $Ex_{ph}$ and chemical exergy $Ex_c$, as shown in Eq. (9).

$$Ex = Ex_k + Ex_p + Ex_{ph} + Ex_c \tag{9}$$

#### 3.1.1. Calculation assumption

The following assumptions are made in the exergy analysis:

1) Assume the components are insulated with environment, and thus there is no heat exergy exchange between the system and external environment;
2) Ignore the potential exergy change of working fluid;
3) Take kinetic exergy of the air entering intake and the gas exiting nozzle into account only, neglecting those of other parts because of the low velocity.

#### 3.1.2. Exergy conservation law for each component

The exergy in the system is corresponding to the entropy, which can change due to entropy flux from outside and entropy production within the system due to irreversible processes: drag losses, heat transfer (not outside, but inside the system from one part of the system to another), chemical transformations, etc. The exergy conservation equation for each component is applied and the results are shown below:

##### 3.1.2.1. Intake.

$$Ex_{in} = \left(Ex_{ph} + Ex_c\right)_{in} + \frac{1}{2}\dot{m}v_{in}^2 = Ex_{out} + \Delta Ex \tag{10}$$

The left part of Eq. (10) is inlet exergy, including physical exergy, chemical exergy and kinetic exergy, and the right part is outlet exergy and exergy loss.

##### 3.1.2.2. Heat exchanger.

$$Ex_{1,in} + Ex_{1,q} = Ex_{1,out} + \Delta Ex_1 \tag{11}$$

$$Ex_{2,in} + Ex_{2,q} = Ex_{2,out} + \Delta Ex_2 \tag{12}$$

Eqs. (11) and (12) are exergy conservation equations for working fluids in heat exchanger, where subscript 1 and 2 denote hot fluid and cold fluid respectively. According to the equation $Ex_{1,q} + Ex_{2,q} = 0$, Eq. (13) is obtained as shown below.

$$Ex_{1,in} + Ex_{2,in} = Ex_{1,out} + Ex_{2,out} + \Delta Ex \tag{13}$$

##### 3.1.2.3. Turbomachinery.

$$Ex_{in} + W_c = Ex_{out} + \Delta Ex \tag{14}$$

$$Ex_{in} = Ex_{out} + W_t + \Delta Ex \tag{15}$$

The exergy conservation equations of turbomachinery are shown in Eqs. (14) and (15), wherein $W_c$ is input power of compressor and $W_t$ is output power of turbine.

##### 3.1.2.4. Turbopump.

$$Ex_{in} + W_p = Ex_{out} + \Delta Ex \tag{16}$$

$W_p$ in Eq. (16) is input power of pump.

##### 3.1.2.5. Combustion chamber.

$$Ex_{in} = Ex_{out} + \Delta Ex \tag{17}$$

Calculation of inlet and outlet exergy in Eq. (17) considers the change of compositions induced by chemical reaction.

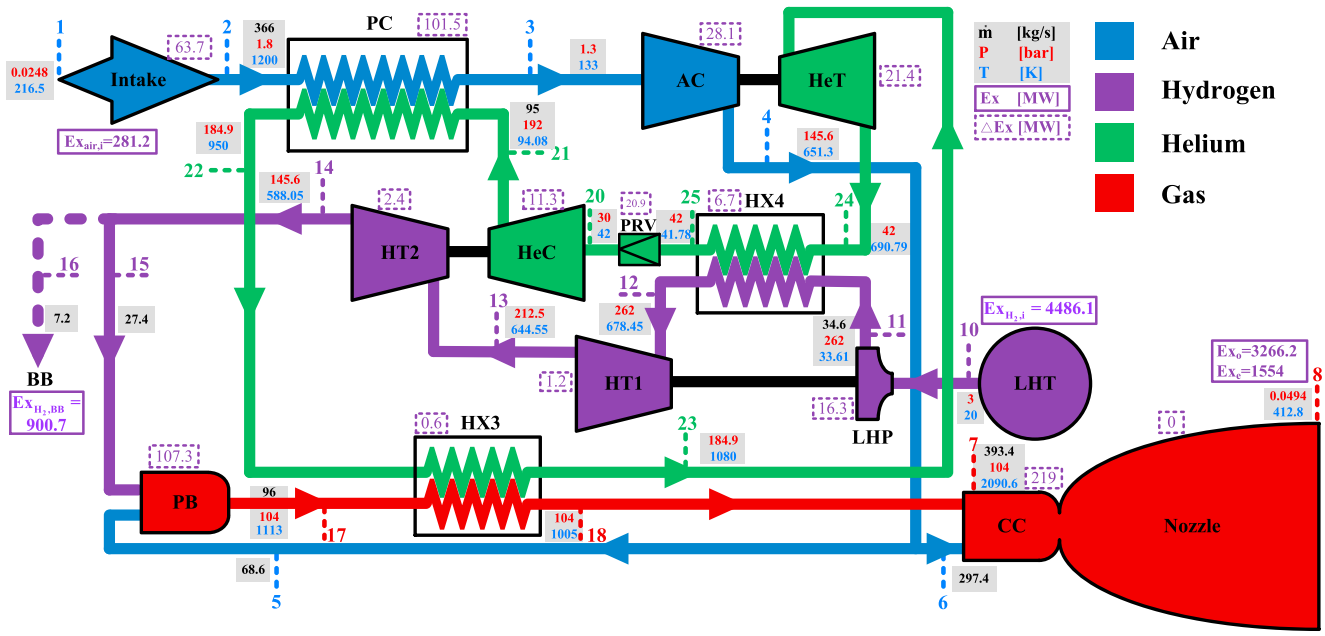


(a)

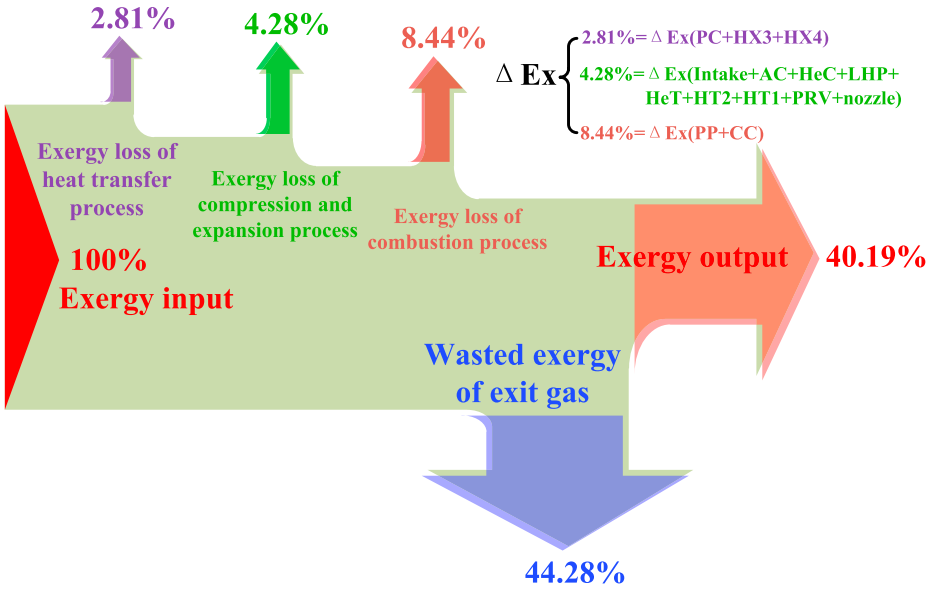


(b)

**Fig. 7.** Exergy analysis of SABRE thermodynamic cycle at design point, (a) exergy parameters of the cycle and (b) exergy flow chart.

*3.1.2.6. Nozzle.*

$$Ex_{in} = Ex_{out} + \Delta Ex = \left(Ex_{ph} + Ex_c\right)_{out} + \frac{1}{2}\dot{m}v_{out}^2 + \Delta Ex \tag{18}$$

The outlet exergy includes physical exergy, chemical exergy and kinetic exergy. The first two parts are wasted and the last part is exergy output of the engine.

*3.1.2.7. PRV.*

$$Ex_{in} = Ex_{out} + \Delta Ex \tag{19}$$

PRV is used to maintain pressure balance for helium loop, then $\Delta Ex$ in Eq. (19) is mainly induced by change of pressure.

By solving equations Eqs. (10)–(19) simultaneously, the cycle exergy efficiency could be obtained as:

$$\eta = \frac{Ex_e}{(Ex_{H_2,in} - Ex_{H_2,BB}) + Ex_{air,in}} = \frac{\frac{1}{2}(\dot{m}_{air} + \dot{m}_{H_2,CE})v_8^2}{(Ex_{10} - Ex_{16}) + Ex_1} \tag{20}$$

In Eq. (20), the denominator is total input exergy of the cycle, which consists of exergy of hydrogen into the cycle and exergy of inlet air respectively. The numerator is the kinetic exergy of exit gas from nozzle, which is the effective exergy of cycle process.

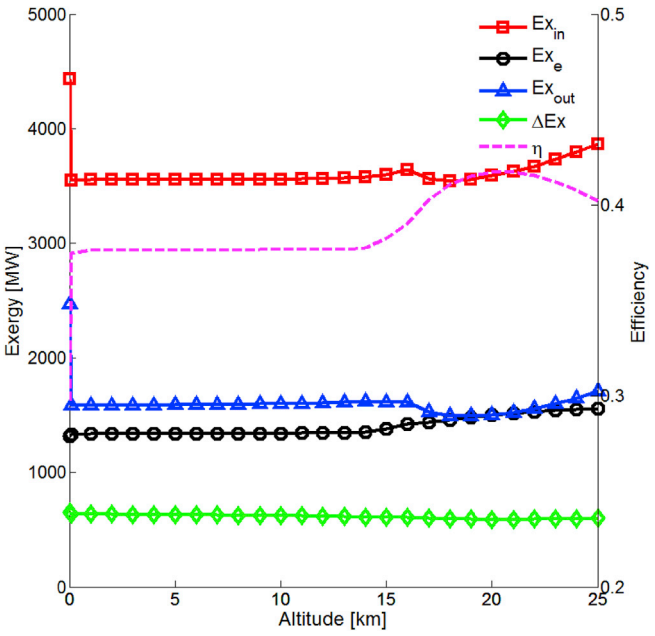


**Fig. 8.** Variation of effective exergy and efficiency along the fight trajectory.

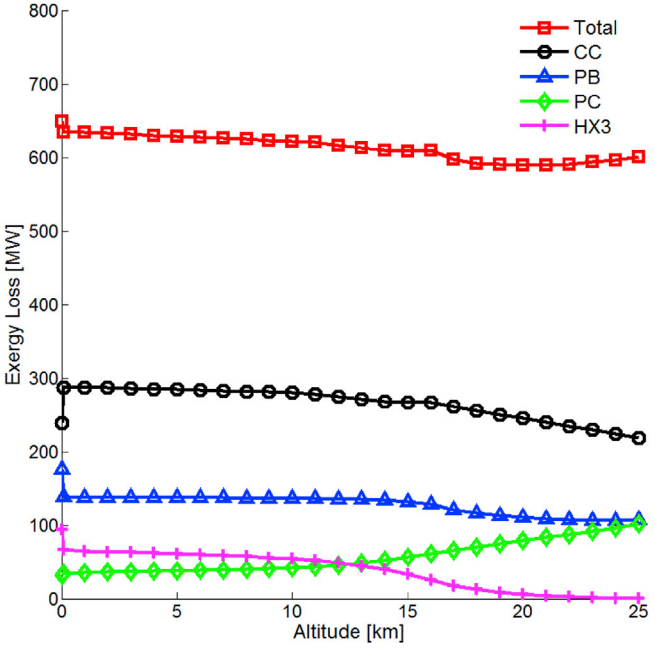


**Fig. 9.** Variation of exergy loss along the fight trajectory.

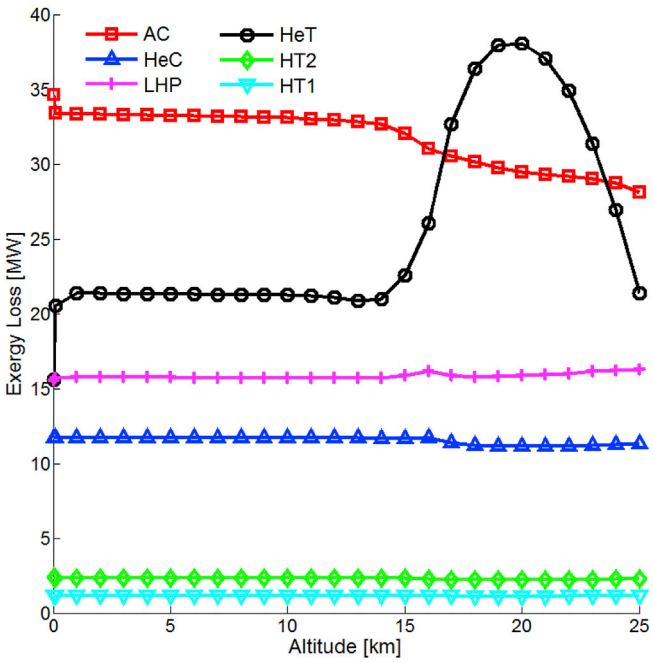


**Fig. 10.** Variation of turbomachinery exergy loss along the fight trajectory.

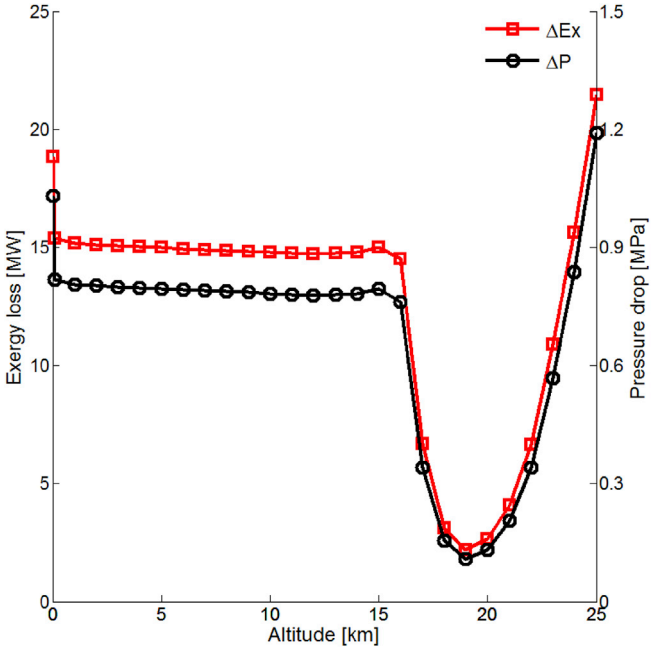


**Fig. 11.** Variation of PRV exergy loss along the fight trajectory.

### 3.2. Result and discussion

Based on the results of cycle parameter in Section 2.3, the exergy flow chart of SABRE at its design point (i.e. 25 km) are obtained, and are shown in Fig. 7. The cycle parameters such as mass flows (black numerals, kg/s), pressures (red numerals, bar) and temperatures (blue numerals, K) are filled with gray background. The exergy flow rate is listed in the solid box, and exergy loss of each component is listed in the dashed box.

Fig. 7(a) shows the exergy input, exergy output of the cycle and the exergy loss of each component. It is indicated that the exergy of inlet air is 281.2 MW. The exergy of hydrogen into the cycle is 4486.1 MW, of which 900.7 MW enters BB. The exergy of exit gas from nozzle is 3266.2 MW, of which 1554 MW is the kinetic exergy. There is exergy loss in each component, which is listed in the dashed box. It is indicated that the total exergy loss around 15.53% of the exergy input, which is produced in these different processes, including heat transfer process, compression and expansion process and combustion process. As shown in Fig. 7(b), exergy loss of these three processes takes 2.81%, 4.28% and 8.44% of the exergy input respectively. Wasted exergy of exit gas consisting of physical exergy and chemical exergy takes 44.28%, which is the biggest part. According to Eq. (20), the cycle efficiency is 40.19%.

Fig. 8 shows the variation curves of effective exergy and efficiency along the flight trajectory. It is indicated that the cycle efficiency is between 29.7% and 41.7%, and greater than 37.4% except for the sea level.

**Table 1**
Optimization results at the altitude of 25 km.

| SN | $A_{PC}$ | $T_{22,max}$ | $T_{23}$ | $T_4$ | $\dot{m}_{He}$ | $\dot{m}_{H_2}$ | $F$ | $Is$ | $\eta$ |
|---|---|---|---|---|---|---|---|---|---|
| | [] | [K] | [K] | [K] | [kg/s] | [kg/s] | [kN] | [m/s] | [] |
| d | $A_0$ | 950 | 1080 | 651 | 95 | 34.6 | 1119.4 | 40876 | 40.19% |
| 1 | $1.05A_0$ | 975 | 1155 | 672.1 | 92 | 33.3 | 1114.4 | 42685 | 41.73% |
| 2 | $1.1A_0$ | 1000 | 1245 | 698.2 | 89 | 32.4 | 1111 | 44058 | 43.25% |

The physical and chemical exergy of exit gas $Ex_{out}$ is greater than 41.8% of the total exergy, which is the biggest part and cannot be used. Since the equivalence ratio is bigger than 1, the wasted exergy is mainly composed by the unburned hydrogen. In order to improve cycle efficiency, it is effective to reduce the equivalence ratio.

There is exergy loss in each component, especially remarkably in CC, PB, PC and HX3. As shown in Fig. 9, more than 71.3% of the total loss is from these four components. It is indicated that loss of combustion process is the biggest part, which is induced mostly by chemical reaction. As the flight altitude increases, the total temperature of air increases rapidly. As a result, the power of heat exchange in PC increases and decreases in HX3 gradually, with the corresponding exergy loss increased and decreased respectively.

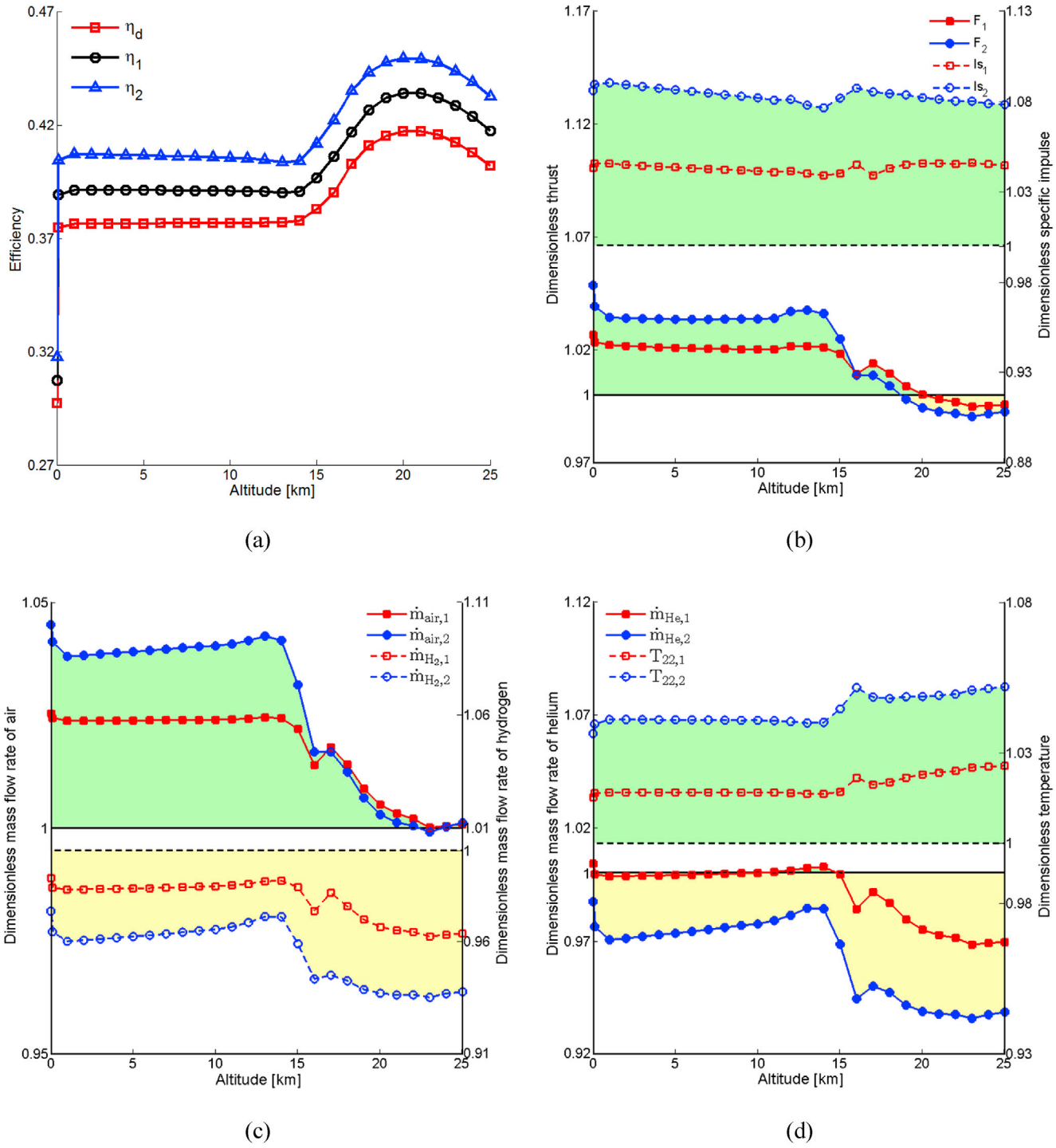


**Fig. 12.** Variation of optimization results along the fight trajectory, subscripts d, 1 and 2 denote SN in Table 1: (a) cycle efficiency, (b) thrust and specific impulse, (c) mass flow rate of propellants, (d) mass flow rate and temperature of helium.

**Table 2**
Result of optimization.

| SN | $W$ [J] | $M_{H_2}$ [kg] |
|---|---|---|
| D | 4.466e11 | 1.932e4 |
| 1 | 4.489e11 | 1.886e4 |
| 2 | 4.487e11 | 1.839e4 |

Fig. 10 shows the variation curves of exergy loss in the turbomachinery along the flight trajectory. It is indicated that the exergy loss in the AC and HeT pair is higher than that in the other turbomachinery, separately, and all of these losses are small. Fig. 11 shows the variation of PRV exergy loss along the fight trajectory. The exergy loss in the PRV is induced by pressure drop, and they are positively correlated to each other. PRV works well with the function of pressure regulation, and only a small exergy loss is introduced.

It is shown that the main exergy loss comes from the unburned hydrogen in exit gas. In other words, a great part of fuel is wasted. In order to improve cycle efficiency, it is necessary to decrease hydrogen flow rate. In other words, it means adjusting to stoichiometric ratio from the current fuel-rich state.

## 4. Optimization of the cycle process

The SABRE cycle is equivalent to the Brayton cycle, thus the equivalence ratio and cycle pressure ratio are the dominant influencing factors of efficiency. In order to improve cycle efficiency, it is also useful to increase the compressor pressure ratio. However, the compressor pressure ratio can only change little in order to adapt the chamber pressure of rocket mode. Therefore equivalence ratio becomes the main factor and the hydrogen flow rate should be decreased.

### 4.1. Optimization of Helium loop

Helium loop is the medium of heat exchange between air and hydrogen. When parameter values of air are determined, the mass flow rate of hydrogen can be regulated by adjusting parameter values of helium loop.

$$(\dot{m}Cp)_{H_2}(T_{12} - T_{11}) = (\dot{m}Cp)_{He}(T_{24} - T_{20}) \tag{21}$$

Eq. (21) shows the energy conservation equation for HX4. According to the actual working process of HX4, temperature difference of helium and hydrogen is basically equal. So the mass flow rate of hydrogen is proportional to that of helium. In order to decrease the equivalence ratio, the mass flow rate of helium should be decreased.

$$W_{HeT} = (\dot{m}Cp)_{He} T_{23} \left(1 - \pi_{HeT}^{\frac{1-k_{He}}{k_{He}}}\right) \eta_{HeT} \tag{22}$$

When the operation parameters of AC are specified, the output power of HeT is determined. According to Eq. (22), it is indicated that helium flow rate decreases as the inlet temperature of HeT or pressure ratio of helium loop increases. As a result, the mass flow rate of hydrogen will be decreased.

$$T_{22} = T_{21} + \frac{(\dot{m}Cp)_{air}(T_2 - T_3)}{(\dot{m}Cp)_{He}} \tag{23}$$

$$(\dot{m}Cp)_{He} \geq \frac{(\dot{m}Cp)_{air}(T_2 - T_3)}{T_{22,max} - T_{21}} \tag{24}$$

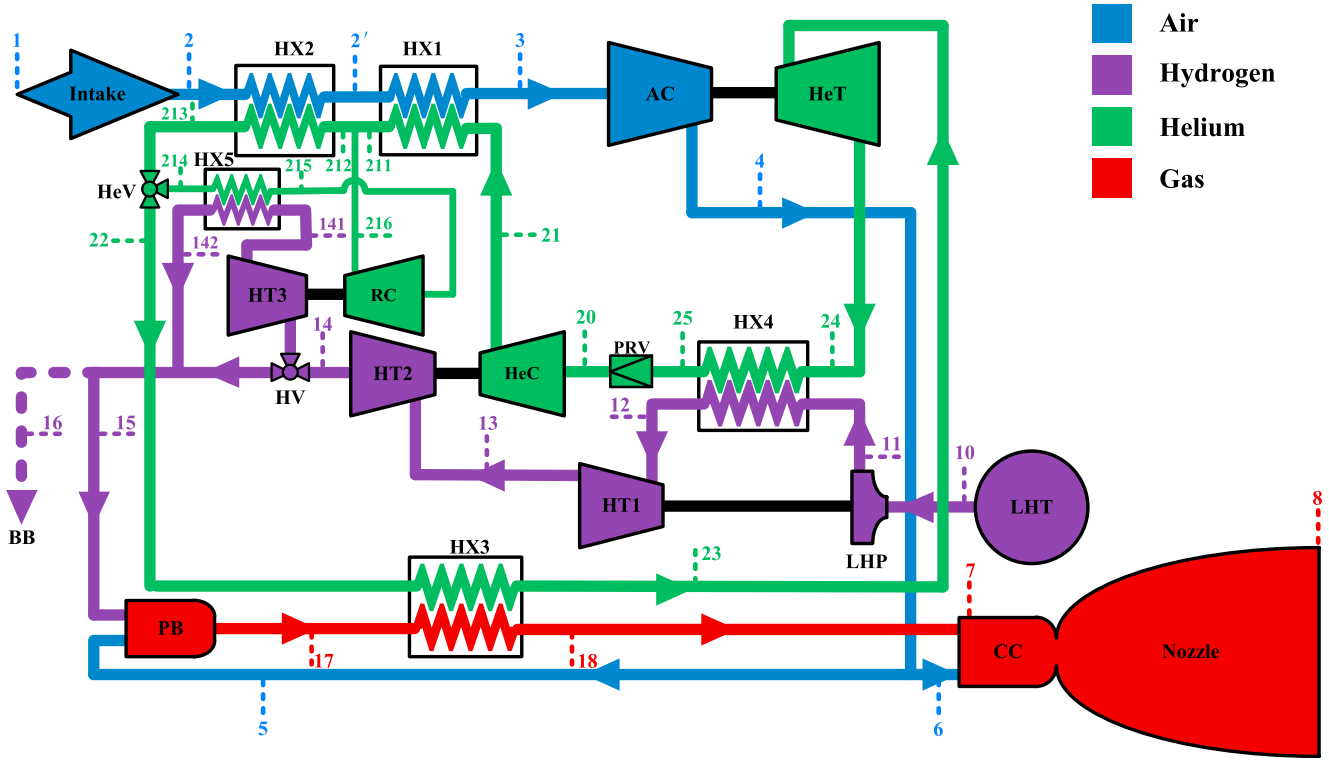


**Fig. 13.** Thermodynamic cycle schematic of helium recirculation scheme.

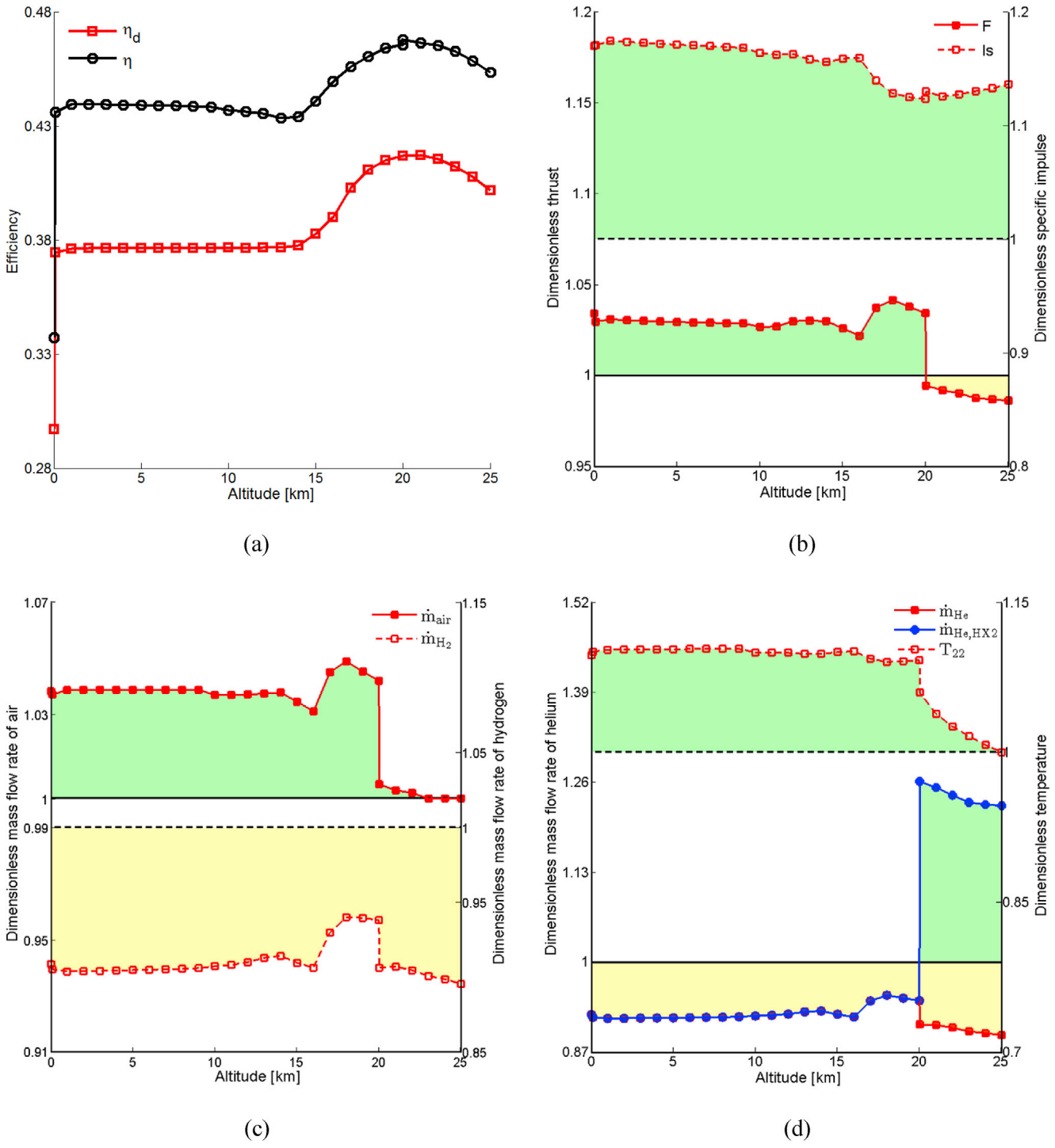


**Fig. 14.** Variation of cycle parameters along the fight trajectory for helium recirculation scheme: (a) cycle efficiency, (b) thrust and specific impulse, (c) mass flow rate of propellants, (d) mass flow rate and temperature of helium.

From the energy conservation equation of PC(see Eq. (23)), it is indicated that as the maximum helium outlet temperature of PC increases, the mass flow rate of helium will be decreased(see Eq. (24)).

It is shown that the mass flow rate of helium will be decreased by increasing the inlet temperature of HeT, pressure ratio of helium loop and the maximum helium outlet temperature of PC. Optimization of helium loop is carried out under a certain limitation of weight and temperature.

$$\begin{cases} A_{PC} \leq 1.2A_0 \\ T_{22} \leq 1000K \\ T_3 \leq 700K \\ T_{23} \leq 1300K \end{cases} \tag{25}$$

As shown in Eq. (25), the limitation includes area of PC $A_{PC}$, helium outlet temperature of PC $T_{22}$, outlet temperature of AC $T_3$ and inlet temperature of HeT $T_{23}$. $A_0$ in the equation is the design area of PC. The pressure ratio of helium loop is kept to be constant due to pressure limitation of the tube of PC.

With the increase of $A_{PC}$, $T_{22}$ and $T_{23}$, $\dot{m}_{He}$ decreases, and so does $\dot{m}_{H_2}$. As shown in Table 1, $T_{22}$ increases to the upper limit (1000 K) firstly, therefore it becomes the actual limitation of the optimization. SN in the table represents the state number, for example "d" denotes the design state which is shown in Sections 2–3. Therefore, state "1" denotes $T_{22,\max} = 975K$, and state "2" denotes $T_{22,\max} = 1000K$.

Fig. 12 shows the variation curves of optimization results along the fight trajectory. The dimensionless parameters are defined to be ratio of actual state and design state, then green region represents bigger parameters than design state and yellow region represents smaller. It is indicated from the results that as $T_{22}$ increases, the helium flow rate decreases(Fig. 12(d)). As a result, the hydrogen flow rate decreases and the air flow rate increases(Fig. 12(c)). In general, the thrust increases except for the high altitude range, and the specific impulse is improved by 8.3% in the trajectory(Fig. 12(b)). The cycle efficiency is advanced by 3% averagely(Fig. 12(a)).

The total work, W (see Eq. (26)), and consumption of hydrogen, $M_{H_2}$ (see Eq. (27)), are calculated to evaluate the general performance in the whole trajectory. The results are listed in Table 2. It is indicated that when $T_{22,\max}$ is increased by 50 K–1000 K, the total assumption of hydrogen will be saved by 4.8%, that's about 930 kg. However, the total work of the engine not only decreases but increases a little. The optimization of helium loop, that is increasing the helium outlet temperature of PC, can effectively improve the cycle efficiency.

$$W = \int FVdt \tag{26}$$

$$M_{H_2} = \int \dot{m}_{H_2} dt \tag{27}$$

### 4.2. Helium recirculation scheme

Though REL proposed the helium recirculation scheme [2], there is not any detail or parameter has been published. The scheme is discussed and performance parameters are calculated in this section.

Fig. 13 shows the thermodynamic cycle schematic of helium recirculation scheme. PC is separated into low-temperature part HX1 and high-temperature part HX2, and the helium recirculator (RC) is equipped, but only work with the flight altitude is above to 20 km. When above 20 km, helium valve(HeV) and hydrogen valve(HV) are switched and RC starts to work. Part of helium out of HX2 enters HX5 and is cooled by hydrogen, then enters HX2 again through RC. At the same time, hydrogen from HT2 flows through 3# hydrogen turbine(HT3) and HX5 in turn before entering PB. As a result, the local helium flow rate of HX2 increases and the capability of PC will be improved. The helium outlet temperature of PC is still limited to 950 K.

The variation of cycle parameters for helium recirculation scheme is shown in Fig. 14. At the work range of RC, the local helium flow rate of HX2 is increased by about 24%, but the helium flow rate is decreased by about 10% (see Fig. 14(d)). Even when RC stops working, the helium flow rate still decreases. As a result, the hydrogen flow rate decreases but the air flow rate increases (see Fig. 14(c)). In general, the thrust increases except for the work range of RC, and the specific impulse is improved by 15.3% in the trajectory (Fig. 14(b)). The cycle efficiency is advanced by 5.6% averagely (Fig. 14(a)).

The total work and consumption of hydrogen are also calculated for the scheme. It is indicated that the total assumption of hydrogen will be saved by 9%, that's about 1740 kg. Meanwhile, the total work of engine is increased by about 1%. The helium recirculation scheme can effectively improve the cycle efficiency.

## 5. Conclusion

This paper carries out efficiency analysis for the deeply precooled combined cycle engine SABRE. A component-level model is developed to calculate the cycle parameters along the trajectory; exergy efficiency analysis is carried out based on the component-level model. Equivalence ratio was determined to be the main influencing factor of cycle, and methods for cycle optimization have been proposed. The main conclusions are as follows.

- Cycle efficiency of the engine is between 29.7% and 41.7% along the trajectory. The wasted exergy at nozzle exit is greater than 37.4% of input exergy, most of which is possessed by the unburned hydrogen;
- There is exergy loss in each component, in particular in CC, PB, PC and HX3. The total losses of these four components is greater than 71.3% of the total loss of the system;
- Equivalence ratio is the major influencing factor of cycle efficiency. The mass flow rate of hydrogen is proportional to that of helium, thus it can be regulated by adjusting parameters of helium loop;
- By increasing the maximum helium outlet temperature of PC by 50 K, the mass flow rate of helium will be decreased. As a result, the total assumption of hydrogen will be saved by 4.8%, that's about 930 kg. The specific impulse is improved by 8.3% in the whole trajectory and the cycle efficiency is advanced by 3% averagely;
- Helium recirculation scheme is an effective method to improve the cycle efficiency. It introduces a helium recirculation loop to increase the local helium flow rate of PC, however helium flow rate of the main loop will be decreased. As a result, the total assumption of hydrogen will be saved by 9%, that's about 1740 kg. The specific impulse is improved by 15.3% in the trajectory and the cycle efficiency is advanced by 5.6% averagely.

## Acknowledgements

The authors would like to express their thanks for the support from the Program for New Century Excellent Talents in University (NCET-13-0156).

## References

[1] R. Varvill, A. Bond, A comparison of propulsion concepts for SSTO reusable launchers, J. Br. Interplanet. Soc. 56 (2003) 108–117.
[2] SKYLON Assessment Report, European Space Agency, 2011.
[3] R. Longstaff, A. Bond, The SKYLON project, in: 17th AIAA International Space Planes and Hypersonic Systems and Technologies Conference, San Francisco, California, AIAA 2011-2244, 2011.
[4] M. Hempsell, R. Longstaff (Eds.), SKYLON User's Manual, Reaction Engines Limited, 2009.
[5] H. Webber, A. Bond, M. Hempsell, The sensitivity of precooled air-breathing engine performance to heat exchanger design parameters, J. Br. Interplanet. Soc. 60 (2007) 188–196.
[6] M. Hempsell, A phased approach to orbital public access, Acta Astronaut. 66 (2010) 1639–1644.
[7] M. Hempsell, J. Aprea, B. Gallagher, G. Sadlier, A business analysis of a SKYLON-based European launch service operator, Acta Astronaut. 121 (2016) 1–12.
[8] D. Cecere, E. Giacomazzi, A. Ingenito, A review on hydrogen industrial aerospace applications, Int. J. Hydrogen Energy 39 (2014) 10731–10747.
[9] M. Hempsell, A. Bond, Skylon: an example of commercial launcher system development, J. Br. Interplanet. Soc. 67 (2014) 434–439.
[10] D. Sziroczak, H. Smith, A review of design issues specific to hypersonic flight vehicles, Prog. Aerosp. Sci. (2016) 1–28.
[11] D. Wright, Future UK space policy - indications from the UK space conference 2011, Space Policy 28 (2012) 50–53.
[12] R.E. Ltd., The SABRE engine, in, http://www.reactionengines.co.uk/sabre.html.
[13] M. Hempsell, A. Bond, R. Varvill, R. Bond, Progress on the SKYLON and SABRE development programme, in: 62nd International Astronautical Congress 2011, Cape Town, South Africa, 2011, pp. 7519–7525.
[14] M. Hempsell, Progress on SKYLON and SABRE, in: 64th International Astronautical Congress 2013, Beijing, China, 2013, pp. 8427–8440.
[15] H. Webber, S. Feast, A. Bond, Heat exchanger design in combined cycle engines, in: 59th International Astronautical Congress, Glasgow, Scotland, 2008.
[16] R. Varvill, Heat exchanger development at Rection Engines Ltd, in: 59th International Astronautical Congress, Glasgrow, Scotland, 2008.
[17] Z.G. Wang, Y. Wang, J.Q. Zhang, B.C. Zhang, Overview of the key technologies of combined cycle engine precooling systems and the advanced applications of microchannel heat transfer, Aerosp. Sci. Technol. 39 (2014) 31–39.
[18] V.F. Villacé, G. Paniagua, Simulation of a combined cycle for high speed propulsion, in: 48th AIAA Aerospace Sciences Meeting Including the New Horizons Forum and Aerospace Exposition, Orlando, Florida, AIAA 2010-1125, 2010.

[19] V.F. Villace, G. Paniagua, Numerical model of a variable-combined-cycle engine for dual subsonic and supersonic cruise, Energies 6 (2013) 839–870.
[20] J. Li, Component modeling and system balance calculation of precooled combined cycle engine under air-breathing mode, in: 2014 academic Conference of China Aerospace Society on Liquid and Special Propulsion Technology, 2014, pp. 82–91.
[21] V.F. Villacé, G. Paniagua, On the exergetic effectiveness of combined-cycle engines for high speed propulsion, Energy 51 (2013) 382–394.
[22] V. Amati, C. Bruno, D. Simone, E. Sciubba, Exergy analysis of hypersonic propulsion systems: performance comparison of two different scramjet configurations at cruise conditions, Energy 33 (2008) 116–129.
[23] O. Balli, A. Hepbasli, Energetic and exergetic analyses of T56 turboprop engine, Energy Convers. Manag. 73 (2013) 106–120.
[24] M.A. Ehyaei, A. Anjiridezfuli, M.A. Rosen, Exergetic analysis of an aircraft turbojet engine with an afterburner, Therm. Sci. 17 (2013) 1181–1194.
[25] N. Kaya, O. Turan, A. Midilli, T.H. Karakoc, Exergetic sustainability improvement potentials of a hydrogen fuelled turbofan engine UAV by heating its fuel with exhaust gasses, Int. J. Hydrogen Energy 41 (2016) 8307–8322.
[26] Q.C. Yang, W. Shi, J.T. Chang, W. Bao, Maximum thrust for the rocket-ejector mode of the hydrogen fueled rocket-based combined cycle engine, Int. J. Hydrogen Energy 40 (2015) 3771–3776.
[27] Q.C. Yang, J.T. Chang, D. Zhang, J.C. Hu, W. Bao, Comment on "Parametric ideal scramjet cycle analysis", J. Thermophys. Heat Transf. 29 (2015) 203–204.
[28] R.F. Cao, J.T. Chang, J.F. Tang, Z.Q. Wang, D.R. Yu, Study on combustion mode transition of hydrogen fueled dual-mode scramjet engine based on thermodynamic cycle analysis, Int. J. Hydrogen Energy 39 (2014) 21251–21258.
[29] J.T. Chang, S.B. Cao, J.L. Zhang, J.F. Z, W. Bao, W.Q. S , Z.X. Li, Effects of air Vitiation on scramjet performance based on thermodynamic cycle analysis, JAAE Open Access 3 (2014).
[30] Y. Ra, R.D. Reitz, A combustion model for IC engine combustion simulations with multi-component fuels, Combust. Flame 158 (2011) 69–90.
[31] R. May, J. Csank, T. Lavelle, J. Litt, T.H. Guo, A high-fidelity simulation of a generic commercial aircraft engine and controller, in: 46th AIAA/ASME/SAE/ASEE Joint Propulsion Conference & Exhibit, Nashville, TN, AIAA 2010-6630, 2010.
[32] W.X. Zhou, J.Q. Huang, Research on the startup model of turbofan engine at high altitude, J. Aerosp. Power 22 (2007) 1384–1390.
[33] G.Q. Luo, Z.C. Sang, R.G. Wang, K.H. Gao, Numerical Methods for Aviation Gas Turbine Engine Simulation, National Defense Industry Press, Beijing, 2007.
[34] L.J. Yang, Q.F. Fu, Design of Liquid Rocket Engine Thrust Chamber, Beijing University of Aeronautics and Astronautics, Beijing, 2013.
[35] S.M. Yang, W.Q. Tao, Heat Transfer, High Education Press, Beijing, 2006.
[36] G.P. Sutton, O. Biblarz, Rocket Engine Foundation, Science Press, Beijing, 2003.
[37] Cantera, in, http://www.cantera.org/docs/sphinx/html/index.html.
[38] K. Liu, Y.L. Zhang, A novel method of calculating the density and temperature of cryogenic propellant rocket engine pump exit, Cryog. Eng. (4) (2002).
[39] N.N. Smirnov, V.B. Betelin, V.F. Nikitin, Y.G. Phylippov, J. Koo, Detonation engine fed by acetylene-oxygen mixture, Acta Astronaut. 104 (2014) 134–146.
[40] N.N. Smirnov, V.F. Nikitin, Modeling and simulation of hydrogen combustion in engines, Int. J. Hydrogen Energy 39 (2014) 1122–1134.
[41] J.Z. Zhou, W.Q. Liu, Z.W. Wang, Engineering Thermodynamics, National University of Defense Technology Press, Changsha, 1999.
[42] H. Kameyama, K. Yoshida, S. Yamauchi, K. Fueki, Evaluation of reference exergies for the elements, Appl. Energy 11 (1982) 69–83.